REVISTA DE METALURGIA, 46 (4)
JULIO-AGOSTO, 320-330, 2010
ISSN: 0034-8570
eISSN: 1988-4222
doi: 10.3989/revmetalm.0939

Microstructural analysis as the indicator for suitability of weld repairing of the heat resistant Cr - Ni steel(•)

Z. Odanović*, I. Blačić**, D. Vračarić**, V. Grabulov*, M. Burzić*** and B. Katavić***

Abstract

Metallurgical evaluation was performed on a fractured column tube of the reformer furnace in an ammonia plant. The tubes were manufactured from centrifugally cast heat resistant steel HK 40. Optical and scanning electron microscope (SEM) were used for microstructural and fracture analysis. For composition determination of the microconstituents energy dispersive X ray spectroscopy (EDS) was used. To evaluate mechanical properties, hardness and microhardness measurements were performed. Investigations based on the microstructural features with the idea to indicate suitability of weld repair of the column were performed in this study. It was observed that the crack initiation, caused by oxidation/corrosion and thermal stresses induced by temperature gradient, appeared in the inner side of the tube wall and propagation occurred along grain boundaries. The results clearly showed the presence of an irregular microstructure which contributed to crack propagation through the tube wall. An occurrence of precipitated needle-shaped carbides/carbonitrides and brittle σ phase was also identified in the microstructure. Results of the microstructural and fracture analysis clearly indicate that reformer furnace columns made of heat resistant steel HK 40 were unsuitable for weld repair.

Keywords

Mrostructural evaluation; Fracture analysis; Steel HK40; Weld repair.

Análisis micro estructural como indicador de la idoneidad de reparación por soldadura de aceros al Cr-Ni resistentes al calor

Resumen

La evaluación metalúrgica se realizó en un tubo de columna con fracturas, que es parte del horno reformador en una planta de amoníaco. Estos tubos son fundidos centrífugamente y fabricados en acero resistente al calor, de tipo HK-40. Para el análisis microestructural de la fractura se ha utilizado microscopía óptica y electrónica de barrido (SEM). La composición de los micro-constituyentes se determinó por espectrometría de rayos X de energía dispersiva (EDS). Las propiedades mecánicas se evaluaron mediante mediciones de microdureza Vickers. Las investigaciones en este estudio se han llevado a cabo con el fin de demostrar la idoneidad de reparación por soldadura de columnas en base a sus características micro-estructurales. Se ha observado que el inicio de la rotura, causada por el efecto de la oxidación/corrosión y el choque térmico ocasionado por el gradiente de temperatura, aparece en la pared interna del tubo y se propaga a lo largo de los bordes de grano. Los resultados demuestran la presencia de una microestructura irregular que contribuyó a la propagación de la rotura a lo largo de la pared del tubo. En la microestructura también se ha registrado la formación da la precipitación de fases de carburo/carbón nitrito que aparecen en forma de agujas y fase σ frágil. Con base en los resultados obtenidos, se puede concluir que la microestructura investigada no es idónea para aplicar la reparación por soldadura.

Palabras clave

Evaluación microestructural; Análisis de fractura; Acero de tipo HK40; Reparación por soldadura.

1. INTRODUCTION

The reformer furnaces are common and critical equipment widely used in the petrochemical industry to produce hydrogen from hydrocarbons in reaction with the steam. The process is performed under operating parameters of high temperatures and high pressures. As a result a most aggressive environment is formed and detrimental mechanims such as oxidation, ageing, carburization and nitriding severely attack the furnace materials. The most critical components of a reformer furnace are

(•) Trabajo recibido el día 6 de Agosto de 2009 y aceptado en su forma final el día 17 de Mayo de 2010.
* IMS Institute, Bulevar vojvode Mišića 43, 11000 Belgrade, Serbia. *zoran.odanovic@institutims.rs; odanovic@ptt.rs.*
** Military Institute of Technology, Ratka Resanovića 1, 11000 Belgrade, Serbia.
*** Institute Goša, Milana Rakića 35, 11000 Belgrade, Serbia.

the columns. The dimensions of the columns vary between 10 and 15 m in height, 100 to 200 mm in diameter and 10 to 25 mm in wall thickness. They are designed for nominal life of exploitation of approximately 100,000 h. The radiant sections of these furnaces operate at temperatures up to 1,150 °C and, because of these extreme temperatures, a highly alloyed heat resistant steel is required. An austenitic steel designated as HK 40 with 25Cr, 20Ni, 0.4C (in wt. %) is mostly used in these furnaces. Since this type of steel cannot be easily drawn or extruded, a centrifugal casting process is used for production of reformer tubes. The furnace columns are formed from the tubes by welding. Damages of the furnace columns may be produced by creep, carburization, thermal shocks and accidental overheating. Replacement of these columns is expensive and difficult compared to other furnace components. These heat resistant cast austenitic materials are characterized by a lack of weldability which is caused by the low ductility due to formation of brittle carbides and nitrides. A lot of trials and errors are involved when it is necessary to repair welds of these tubes. In some cases weld repair is impossible, or repair is not recommended[1-5].

Systematic studies have previously been carried out to define preferential sites for damage accumulation and to explain damage morphology of fractured columns and other failed components of the reformer furnace. They showed that fracture analysis could be applied to assess reformer column and furnace components safe life and to ensure in advance the planning of component replacement in order to avoid unplanned shutdowns during the campaign. Other studies dealt with different weld repair strategies which were proposed and applied[1 and 3].

There are no adequate studies in the literature aimed at correlating the fracture analysis with suitability of weld repair. In this study a fracture analysis was performed and microstructural features of the fractured column of the reformer furnace were analyzed with the idea to indicate the suitability of weld repair of the reformer column.

2. EXPERIMENTAL

2.1. Material

The investigations were performed on the tube made of centrifugally cast, heat resistant, steel HK 40. Chemical composition and mechanical properties of the steel are presented in tables I and II, respectively[6 and 7]. The tube was operated for 55,000 h prior to failure. The diameter of the investigated tube was 114.8 mm and the wall thickness, 21.85 mm.

The fracture location of the damaged primary reformer is schematically shown in figure 1. Microstructural investigations of the material were performed on the segment near the location of fracture, designated as A, whereas the segment B on the other part of the reformer tube, where possible deformation did not occur, served as a reference sample. Segment A was collected from the part beneath the roof, while segment B was sampled from the location above the collector.

2.2. Testing

Macro and microstructural examinations in longitudinal direction and perpendicular to the tube axis were performed. Schematic presentation of the tested positions of the segments A and B are shown in figures 1 b) and c), respectively. Surfaces marked in figure 1, were grinded, polished and etched by the standard procedure prior to examination by optical microscope. The etchant was *Aqua regia*. Measurement of oxidized layer depth and the porosity share were performed as an integral part of all metallographic examinations. Investigated fractured surfaces of the tube are presented in figure 2.

The surfaces of the failure without previous preparation were analyzed visually and by scanning electron microscope (SEM), while samples for microstructural investigation by SEM were prepared by polishing and etching. A qualitative analysis of microstructure was performed by energy dispersive X ray spectroscope (EDS) in order to establish the composition of chemical microconstituents.

Table I. Chemical composition of the investigated steel [wt. %] [6]

Tabla I. Composición química del acero investigado [% en peso][6]

C	Mn	Si	Cr	Ni	P	S	Mo	Fe
0.35-0.45	0.40-1.50	0.50-1.50	23.00-27.00	19.00-22.00	<0.03	<0.03	< 0.50	rest

Table II. Mechanical properties of the investigated steel at room temperature[7]

Tabla II. Propiedades mecánicas a temperatura ambiente del acero investigado[7]

Properties	Min.
Tensile Strength, Rm, [MPa]	450
Yield Strength, Rp, [MPa]	240
Elongation A5, [%]	15

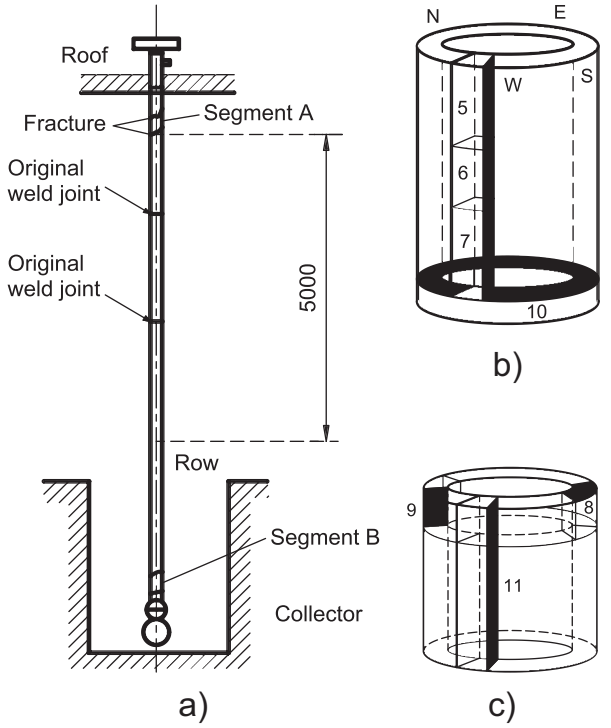

Figure 1. Schematic presentation of the primary reformer with tested segments designated as A and B. a) Location of the tested segments; b) Analyzed cross sections (gray) of segment A where fracture occurred; c) Segment B above collector with analysed sections.

Figura 1. Presentación esquemática del principal horno reformador con segmentos examinados, designados como A y B. a) Posición de los segmentos examinados; b) Secciones analizadas (gris) del segmento A donde apareció la fractura; c) Segmento B por encima del colector con secciones analizadas.

Brinell hardness measurements (HB 5/750/20) were performed on the tube wall cross section to evaluate mechanical strength and to determine a possible carburisation/decarburisation. Microhardness measurements were performed by Vickers method applying a load of 25g ($HV_{0,025}$) for hardness determination of the particular microconstituents.

3. RESULTS

3.1. Macrostructure

The fractured surface of the cross section of the failed tube from the upper segment A is shown in figure 2 a). Radial ridges are clearly visible, forming chevron marks of fracture pointed toward the fracture area. Dark regions near the inner and outer surfaces of the tube, with ridges pointed toward mid-wall thickness are also visible. It was found that the initial crack was originated on the inner side of the tube and marked as "F". This crack was afterwards opened by additional deformation. The features of the fractured surfaces, in the longitudinal direction of the tube, are presented in fgure 2 b) and denoted as FS. Two distinctive areas are clearly visible: a dark, semicircular area with an oxide film, and a light area as a result of the fresh crack opening. The crack propagation direction was perpendicular to the tube wall and was branched to the 2/3 of the wall thickness. In this area two zones may be identified. The first zone at the inner wall of the tube, width 2 to 3 mm in thickness, is characterized by unidirectional configuration, whereas the second zone is distinguished by fan-like ridges directed to the inner surface of the tube. According to dark colour (Fig. 2 b)) it could be concluded that this surface was formed before the final fracture of the tube along the tube cross section.

The macrostructure of the tube segments A and B, in both directions, is presented in figures 3 and 4, respectively. Fine equiaxed grains next to the outer tube wall which cover from 1/3 to 2/3 of the wall thickness are shown in figure 3. The columnar structure is only found partially in the microstructure. On the other side, the macrostructure of the tube segment B consists of fine equiaxed grains next to the outer tube wall and coarse undirected grains next to the inner tube wall (Fig. 4). Elongated columnar grains oriented in a radial direction and covering more than 2/3 of the wall thickness are located in the interspaces.

3.2. Microstructure

Microstructural examinations of the segment A of the fractured tube by optical microscope revealed an oxide layer and porosity. The measured depth of oxide layer is about 120 μm at the inner side of the tube. The porosity is continuously and circumferentially dispersed, with

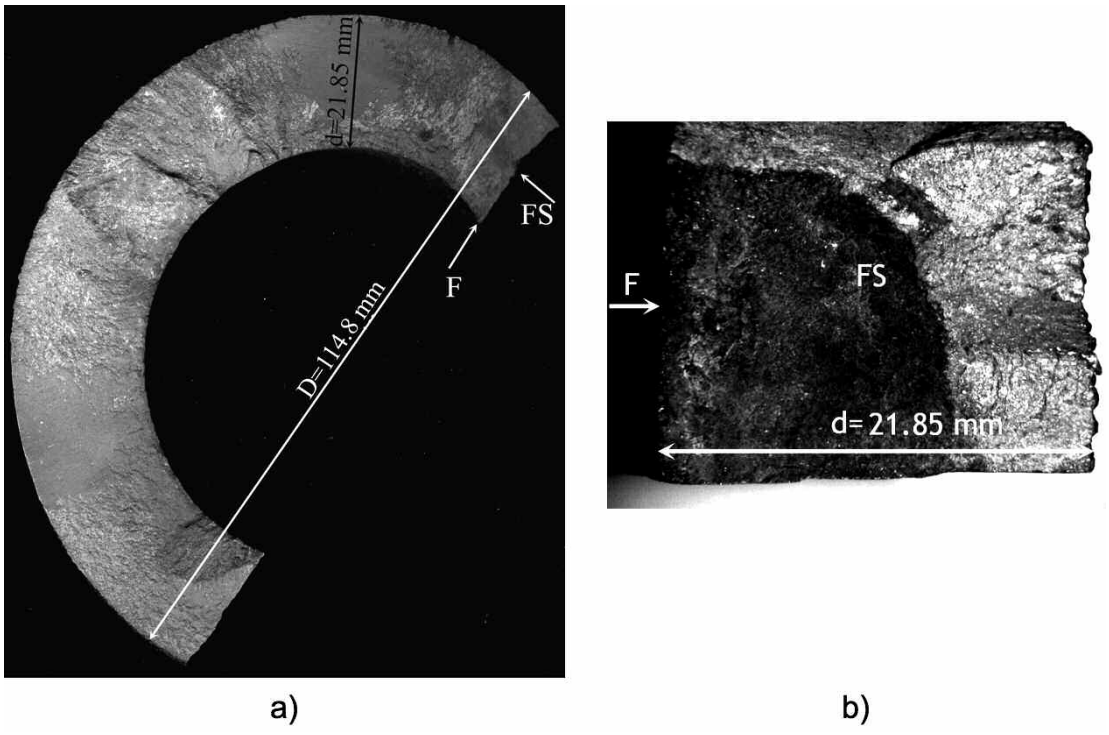

Figure 2. Fractured surface of the tube: a) cross section; b) longitudinal direction. F denotes the location of fracture and FS denotes fractured surface.

Figura 2.Superficie del tubo con fracturas: a) Sección transversal; b) Dirección longitudinal. F denota la ubicación de la fractura y FS denota la superficie con fracturas.

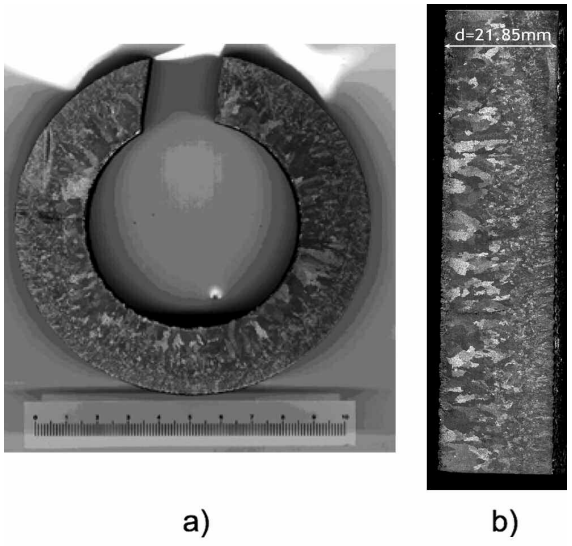

Figure 3. Macrostructure of the segment A. a) cross section of the tube, sample 10; b) longitudinal direction of the tube, sample 5. Etched in the Aqua regia.

Figura 3. Macro estructura del segmento A. a) Sección transversal del tubo, muestra 10; b) Dirección longitudinal del tubo, muestra 5. Desgastada por la presencia de Agua regia.

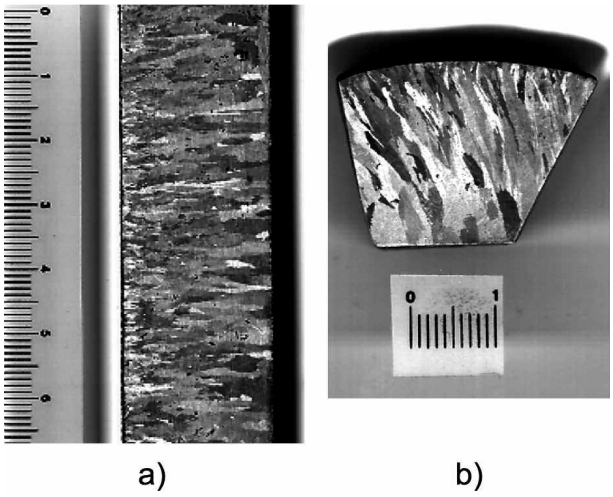

Figure 4. Macrostructure of the segment B above collector. a) longitudinal direction, sample 11; b) tube cross section, sample 8. Etched in the Aqua regia.

Figura 4. La macro estructura del segmento B por encima del collector. a) Dirección longitudinal, muestra 11; b) Sección transversal de tubo, muestra 8. Desgastada por la presencia de Agua regia.

the average depth of 300 µm. The branching of the radial and axial cracks directed from the inner to the outer surface of the tube in the longitudinal sample is illustrated in figure 5 a). It is evident that the cracks are propagated along the grain boundaries of the austenite grains, as shown in figure 5 b). The presence of oxidation and/or carbonization products in the bulk of the crack is visible in figure 5 c) and d) obtained by SEM.

Microstructures of the bulk material from the tube segment A analyzed by light microscope, in cross section and in the longitudinal direction, are presented in figure 6. The microstructure is distinguished by the austenite matrix with precipitated globular eutectic carbides located at grain boundaries, needle-like precipitated carbides and carbonitrides within the grains.

The difference in morphology of carbides precipitated at the grain boundaries at the inner and outer side of the tube wall may be observed. Needle-like precipitates inside the grains from the outer side of the wall are coarser and longer than those at the inner side of the tube. Details of the microstructure analyzed by SEM and EDS are shown in figure 7. The presence of austenite matrix with massive precipitates at the grain boundaries was revealed in figure 7 a). Globular gray phase which could be precipitated σ-phase was evidenced at the grain boundaries. Dispersed secondary needle-shaped carbides/carbonitrides within grains were also identified. EDS analysis of the matrix is shown in figure 7 b). The atomic spectrum of precipitates and grain boundaries is shown in figure 7 c). Precipitates were enriched in Cr and depleted in Ni. The presence of non-metallic

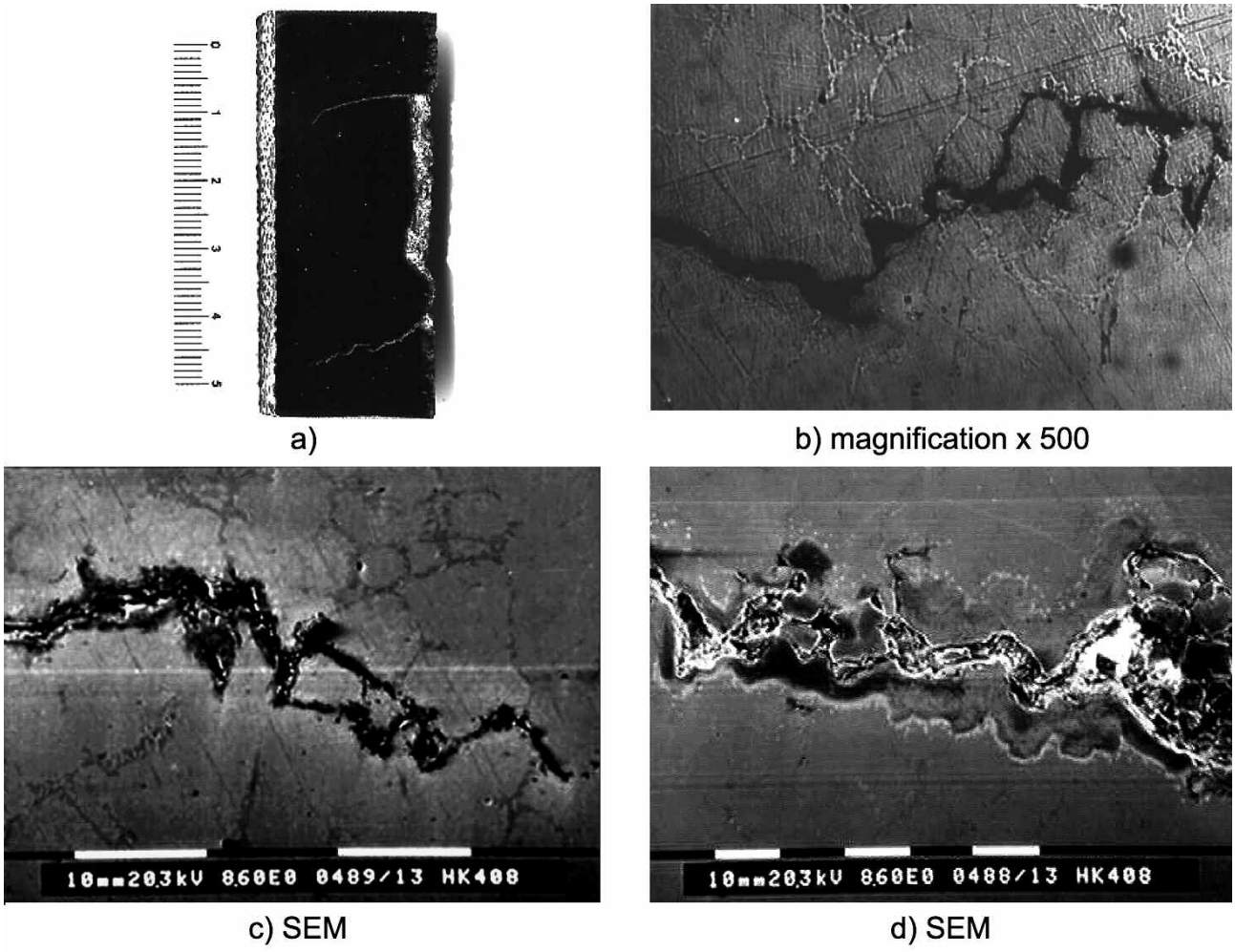

Figure 5. Crack branching from inner to outer side of the tube through the wall thickness. a) Macro view; b) Optical microscope; c) and d) SEM image of the crack end. Polished and etched.

Figura 5. Ramificación de la rotura desde la superficie interior hasta la superficie exterior del tubo a través del espesor de la pared del tubo.a) Vista total; b) Microscopios ópticos; c) y d) SEM ilustración del fin da la rotura, pulido y desgastado.

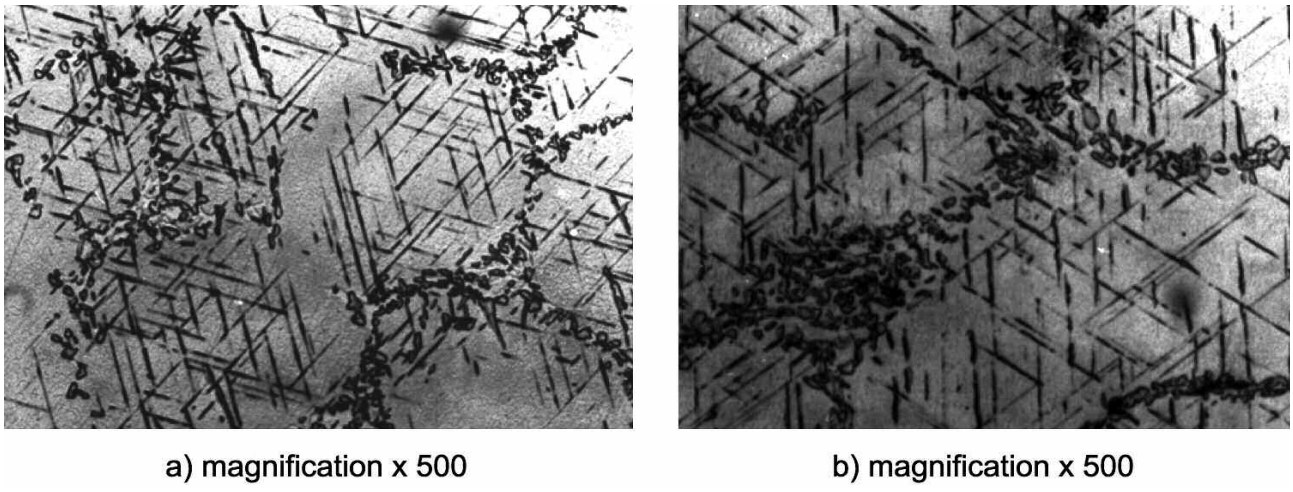

Figure 6. Microstructure of the bulk material from segment A obtained by optical microscope. a) Tube wall cross section; b) Tube wall longitudinal direction. Etched in Aqua regia.

Figura 6. Microestructura del material de segmento A obtenidos por microscopio óptico. a) Sección transversal de la pared del tubo; b) Dirección longitudinal de la pared del tubo, desgastada por la presencia de Agua regia.

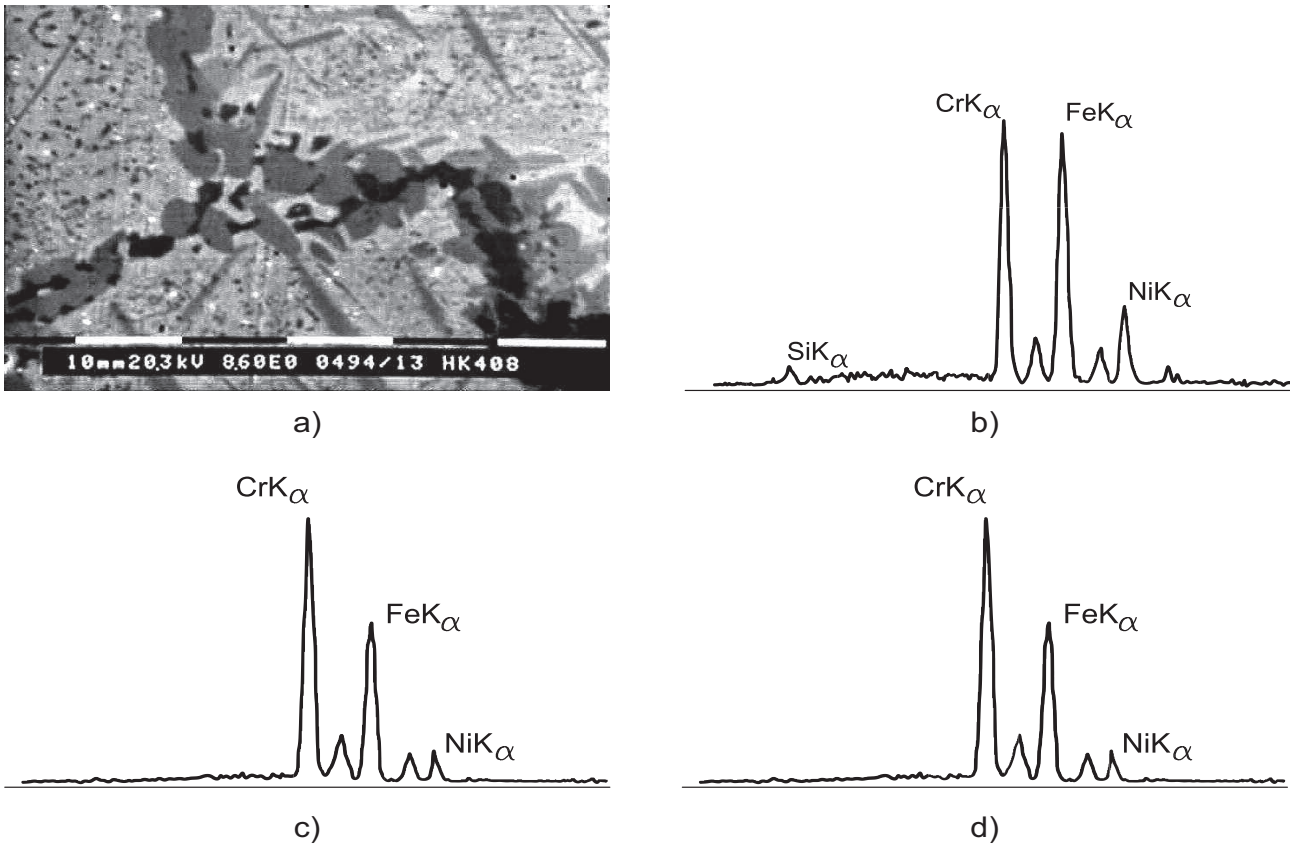

Figure 7. Microstructural analysis of the tube material from fractured segment A. a) SEM; b) EDS analysis of the matrix; c) EDS analysis of the grain boundary - gray phase; d) EDS analysis of the sulphide inclusion - black phase.

Figura 7. Análisis microestructural del material de tubo en el segmento A donde aparece la fractura. a) SEM; b) EDS análisis de la matriz; c) EDS análisis de los bordes de grano - fase gris; d) EDS análisis de la inclusión de sulfuro de – fase negra.

inclusions found as dark phase mainly corresponds to MnS-type inclusions (Fig. 7 d)).

Chemical composition of the matrix and microconstituents is shown in table III. From the ratio of Fe/Cr it could be deduced that these precipitates are carbides, whereas carbides within grains are of M_7C_3-type and the grain boundaries precipitates correspond to σ- phase and M_6C-type carbides[8].

Microstructures of samples from segment B above collector are shown in figure 8. Analysis was performed by optical microscope in longitudinal and transverse direction. The same pattern for sampling areas was applied with sample A. The microstructure is austenite matrix with precipitated eutectic carbide phase dispersed at grain boundaries and fine carbides within grains. The volume fraction of carbides is significantly lower at the grain boundaries compared to carbides within grains. There is no distinct difference of the microstructure in shape, volume and distribution between the inner-side, the mid-wall thickness and the outer-side samples. The same is valid for the longitudinal and transversal directions.

The results of EDS analysis are presented in table IV with approximate chemical composition of matrix, grain boundaries and precipitates in the austenitic matrix. Compared to results of table III,

Table III. Chemical composition of microconstituents of segment A, analyzed by EDS

Tabla III. Composición química de los microconstituyentes en el segmento A, analizada mediante EDS

Phase	Chemical composition in [wt. %]				
	Si	Cr	Ni	Fe	Total
matrix	1.38	32.98	19.11	46.63	100
grain boundary	1.13	54.30	7.91	36.66	100
carbide	1.18	41.42	16.01	41.39	100
needle	1.24	48.31	8.45	43.00	100

Table IV. Chemical composition of microconstituents in segment B, analyzed by EDS

Tabla IV. Composición química de los microconstituyentes en el segmento B, analizada mediante EDS

Phase	Chemical composition in [wt. %]				
	Si	Cr	Ni	Fe	total
matrix	1.22	28.34	20.21	50.23	100
grain boundary	1.11	82.01	4.56	12.32	100
carbide	1.77	72.05	7.44	18.74	100

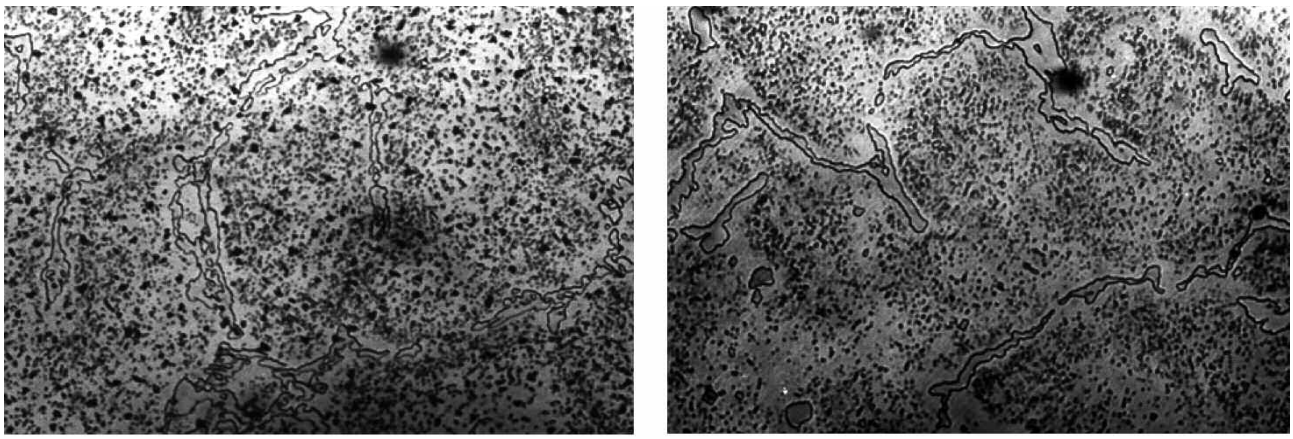

a) magnification x 500 b) magnification x 500

Figure 8. Microstructure of the bulk material from segment B obtained by optical microscope. a) Tube wall cross section, sample 8 from figure 3; b) Tube wall longitudinal direction, sample 9 from figure 1. Etched in Aqua regia.

Figura 8. Microestructura del material del segmento B obtenido mediante microscopio óptico. a) Sección transversal de la pared del tubo, muestra 8 de la figura 3; b) Dirección longitudinal de la pared del tubo, muestra 9 de la figura 1, desgastada por la presencia de Agua regia.

carbide precipitates were highly enriched in Cr and depleted in Ni. Values of chemical composition in table IV indicate that carbides within grains could be defined as of $M_{23}C_6$-type. The same type of carbides is precipitated at the grain boundaries.

The results of the fracture analysis by SEM are shown in figures 9 and 10. The crack initiation site, which is shown in figure 2 b) (segment A) as a dark semicircle surface, is shown in figure 9 a). Spectrum analysis has shown that, besides the expected elements (Fe, Cr, Ni and Si), Al- and Ca-based compounds were also detected. The characteristic fracture surfaces are shown in figure 10. It is evident that the crack was initiated and propagated on the dendrite boundaries where corrosion products were located. The fracture surface where the crack was intergranularly extended along the dendrite grain boundaries is illustrated in figure 10 a), where as figure 10 b) shows an area with presence of secondary cracks. The transition area where a transgranular fracture is found may be seen in figure 10 c). The final opening of the crack by tearing is shown in figure 10 d).

3.3. Macro and microhardness

Results of hardness measurements across the wall thickness of segments A and B (see figure 1) are shown in table V. Analysis of each group of results has shown that there is no distinguished difference in hardness, except on fractured segment A. Namely, near the inner surface somewhat lower hardness of the tube was found. The average hardness of the segment A is high compared to segment B.

The results of microhardness ($HV_{0,025}$) measurements of the same microconstituents of segments A and B are shown in table VI. The values of microhardness corresponding to grain boundaries are higher in segment A compared to segment B. There is no significant difference in microhardness values within matrix grains of both samples.

4. DISCUSSION

The results indicate that the catastrophic failure of the tube was not initiated on the cross section of the wall of the bulk material. The morphology of the fractured surfaces shown in figure 2 is the result of progressive fracture and suggests that it is caused by thermal and mechanical strain. There is no evidence of creep or fatigue damage during service life. The analysis of longitudinal fractured surfaces reveals that the crack growth was a long-time process and was initiated on highly oxidized surfaces at the inner side of the wall. It could be concluded that crack growth was induced by thermal strains as a result of a temperature gradient along the wall thickness of the tube. Also, it is highly possible that thermal shock has to be taken into account as a support for the crack propagation.

Macrostructural characteristics of segment A (Fig. 3) cannot meet the requirements proposed for sound cast structure. For this particular purpose such macrostructure must have fine equiaxed grains on the outer side of tube wall, coarse equiaxed grains near the inner side of the tube, and elongated columnar grains between these two regions. The

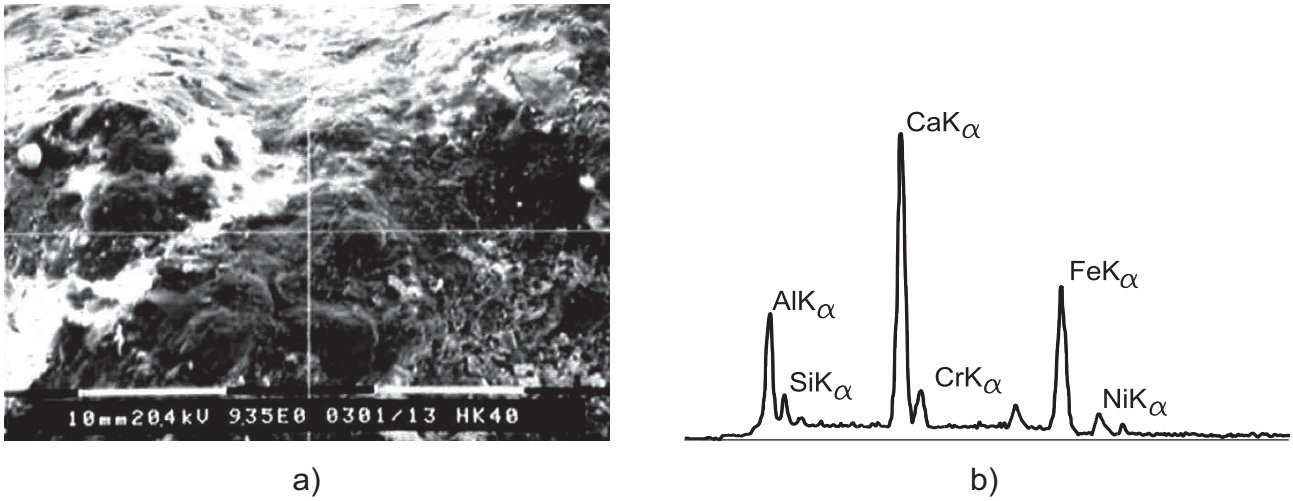

Figure 9. Image of the fracture initiation. a) SEM; b) EDS analysis of corrosion products.

Figura 9. Imagen del inicio de la rotura. a) SEM; b) EDS análisis de productos de corrosión.

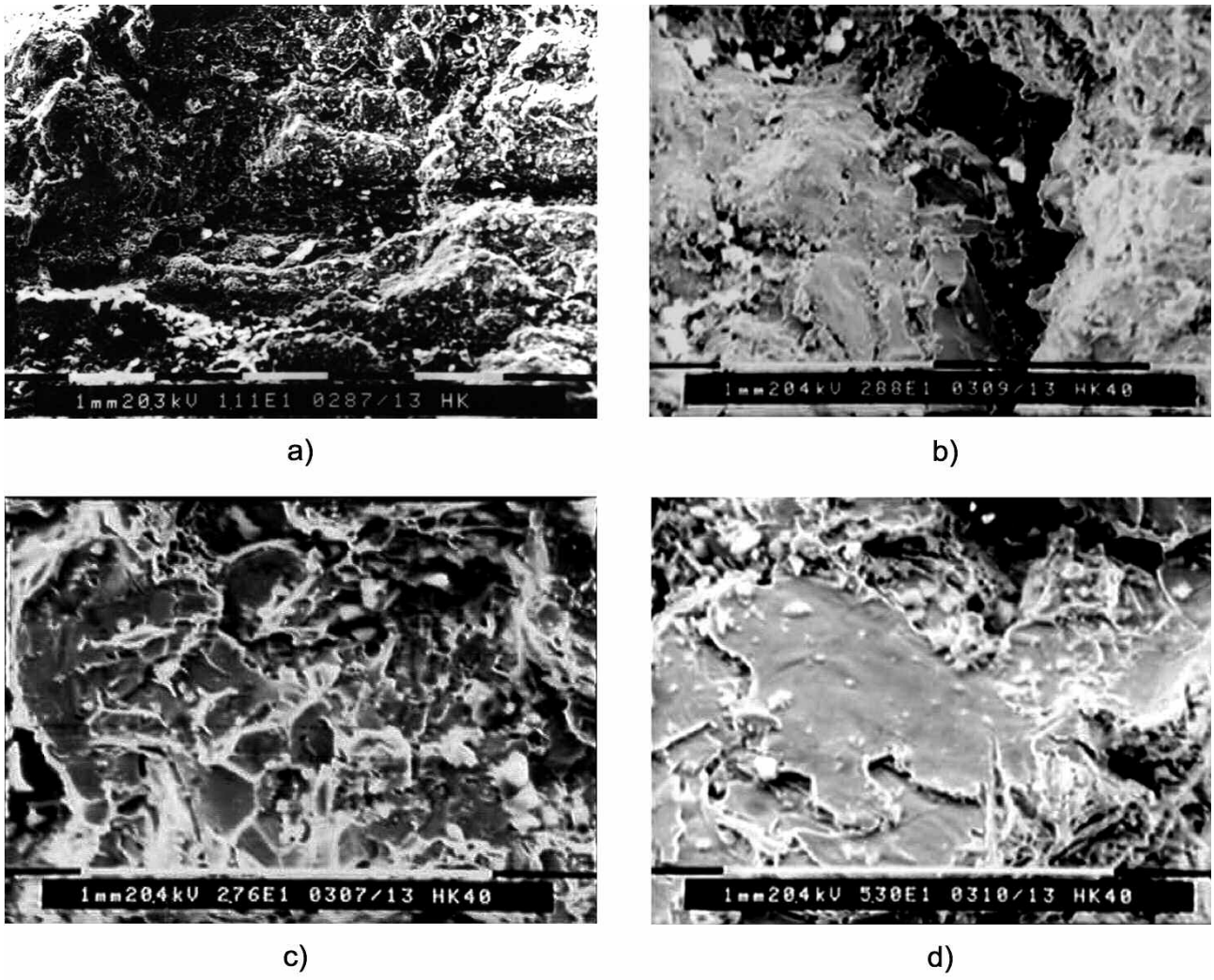

Figure 10. SEM images of the fractured tube. a) Surfaces with crack extended along dendrite grain boundaries – intergranularly; b) Area with the presence of secondary cracks; c) Final stage of transgranular fracture; d) Surface of the crack opening by tearing.

Figura 10. SEM ilustraciones de tubo con fracturas. a) Superficies con fracturas que se propagan a lo largo de los bordes dendríticos del grano – intergranular; b) Áreas con grietas secundarias; c) Fase final de la grieta transgranular; d) Superficie de la grieta originada por desgarro.

shape, size, orientation and proportion of the columnar grains play an important role in the fracture resistance of the steel. The zone with elongated columnar grains should be more than half of the wall thickness[2]. In the case of this class of high-temperature steels, cracks spread intercrystallinically and in this case the size, shape and orientation of grains have a dominant influence on crack growth. These factors, as well as the fraction of elongated columnar grains, are the result of casting and solidification conditions[1-4]. As a result of improper centrifugal casting and solidification processes, an irregular macrostructure with majority of equiaxed crystals without elongated columnar crystals zone was detected. These facts eliminate the macrostructure of the segment A as suitable for weld repair. On the other side, macrostructure of segment B is in accordance with requirements for recommended macrostructure.

Porosity and oxidation were identified at tested segments. Also, the thickness of the oxidized layer accompanied with porosity is relatively small. Thus, these factors probably cannot play a significant role in deterioration of the tube material properties and they are not of importance for weld repair[1-3].

Besides the difference in macrostructure, a difference in microstructure of the tested segments A and B (Figs. 6 and 8) was also identified. The

Table V. Hardness results measured across the wall thickness

Tabla V. Resultados de dureza medida a través de la pared

segment	Distance from the inner wall surface, mm	2.0	4.5	7.8	10.0	13.1	16.5	19.0	mean value
A	Hardness, HB5/750/20	255	288	285	285	295	302	295	286
segment	Distance from the inner wall surface, mm	3.2	5.5	10.5	11.0	12.0	16.2	17.0	mean value
B	Hardness, HB5/750/20	185	200	191	195	185	191	185	190

Table VI. Microhardness of the microconstituents in the structure

Tabla VI. Microdureza de los microconstituyentes en la estructura

Sample	Location	$HV_{0.025}$			mean value $HV_{0.025}$
segment A	grain boundary	315	397	493	401
	grain	178	151	203	177
segment B	grain boundary	320	243	247	270
	grain	188	193	206	195

microstructure of both segments consists of austenite matrix, with randomly dispersed carbides and/or carbonitrides. Eutectic carbides are located at the grain boundaries. During solidification austenite dendrites were first formed and at the end of the solidification process carbides were precipitated in the interdendritic space creating strings of the grain boundaries[8].

Long-term exposure at high temperature leads to decomposition of austenitic matrix, inducing the carbon precipitation and formation of various types of carbides and intermetallic compounds within grains and at the grain boundaries. Carbides of $M_{23}C_6$ type were transformed to temporary formed M_6C carbides. These carbides reduce ductility and other mechanical properties at high temperatures. During long-time exposure brittle intemetallic phases were also formed, like α-phase, which increases the susceptibility of steel to brittle fracture[8-10]. This kind of microstructural feature is not detrimental for weld repair, as the original ductility can be restored by a high temperature solution annealing.

However, in the microstructure of the segment A, which was operated on the level of the heating burner, pearl-shaped carbides were identified at grain boundaries, which indicates a probable overheating of the tube material above the working temperature. This type of microstructure is regarded as unfavourable for steel weldability. Precipitated needle-shaped carbides/carbonitrides as well as brittle σ- phase at grain boundaries and within grains (Figs. 6 and 7) were also identified in the microstructure. The results of the microhardness measurements identified the presence of precipitates with higher hardness at grain boundaries of the segment A. The fact that the difference exists between microstructures of segment A and B is confirmed by results of hardness testing (Table V) with significantly higher values of segment A hardness. The presence of the needle-shaped high hardness precipitates, causing brittleness of the material, intensively reduces weldability. The morphology and high hardness of the microconstituents in the microstructure of the segment A indicates that solution annealing before welding could not recover the microstructure for weld repair.

The results of the fractured surface analysis presented in figures 9-10 could be used for explanation

of the fracture initiation and propagation mechanisms. The fracture was initiated on oxidation/corrosion products from the inner side of the tube wall. The crack propagates intercrystally, i.e. along the grain boundaries of fine dendrites. Secondary cracks were also identified, as shown in figure 10. The final stage of fracture was of the cleavage type, when the crack propagates transcristally. The presence of oxidation/corrosion products in the material of the segment A, the existence of fine dendrites without columnar structure, and the occurrence of the secondary cracks, deteriorate weldability, giving the evidence that the investigated material is unsuitable for weld repair.

5. CONCLUSIONS

In spite of the limiting potentials imposed by optical and scanning electron microscopy, and absence of mechanical and/or fracture mechanics tests, the results of this study have clearly demonstrated the origin of fracture of a reformer tube made of heat resistant Cr-Ni (HK 40) steel. Results of the microstructure and fracture analysis have proven to be a powerful indicator about suitability of weld repair of the fractured tube.

Crack initiation appeared at the inner side of the tube wall and was enhanced by oxidation/corrosion. As a consequence of the temperature gradient induced by thermal stresses and possible malfunction of the power plant, crack propagates along brittle grain boundaries through wall thickness. Morphology and distribution of present microconstituents indicate a possible overheating of tubes above operating temperature which enhanced crack growth. On the other hand, the appearance of microstructural features during overheating is detrimental for weldability.

The presence of an irregular macrostructure, with majority of equiaxed crystals without elongated columnar crystals zone, as a result of improper centrifugal casting and solidification processes, was also a key factor contributing to a relatively fast crack growth through thickness. Also, these parameters eliminate microstructure of the segment A as suitable for weld repair. The presence of precipitated hard, needle-shaped carbides/carbonitrides, as well as brittle σ- phase at grain boundaries and within grains, gave a strong indication that the investigated microstructure does not meet the requirements for weld repair at the spot of fracture. This structure is not suitable for high temperature heat treatment annealing for recovering and preparing for weld repair. Under these circumstances, the replacement of the whole tube should be recommended.

Acknowledgement

This work was carried out as part of the project 19023: "Development of the new repair welding technologies for intervention maintenance of thermo-energetic plants" supported by the Ministry of Science and Technological Development of the Republic of Serbia.

REFERENCES

[1] T.L. da Silveira. and I.L.May, *Arab. J. Sci. Eng.* 31 (2006) 99-118.
[2] S.M. Zhu, S.J. Zhu and J.S. Zhang, *Mater. Sci. Technol.* 12 (1996) 513-517.
[3] J. Vekeman and M. de Waele, *IIW Doc. IX-2266-08* (2008).
[4] A.U.Hamid and H.M Tawancy, *Eng. Failure Analysis* 13 (2006) 1005-1021.
[5] S.K. Bhaumik and R.Rangaraju, *Eng. Failure Analysis* 9 (2002) 553-561.
[6] *www.kubotametal.com/HR/HK40.ht.*
[7] *Technical specification B14-2M-87R*, *Kellogg*, (1987).
[8] *Metals Handbook*, *Vol. 9*, ASM International, 9th edition, 1987, pp. 177-178.
[9] A.J.P. Tucker., *Ammonia Plant Safety* 14 (1972) 75-84.
[10] K. Guan, H.Xu, Z . Wang, *Eng. Failure Analysis* 12 (2005) 420-431.